An Analytical Mass Spectrometer for the Gas Analysis

AUTHOR(S):

KADOTA, Noriaki; ISHIDA, Seiichi; MASUDA, Yoshihiro

An Analytical Mass Spectrometer for the Gas Analysis

By

Noriaki KADOTA, Seiichi ISHIDA and Yoshihiro MASUDA

Department of Fuel Chemistry

(Received September 6, 1956)

The tentative construction of a mass spectrometer of $\pi/2$ (Hipple type) single magnetic focusing to be used for the gas analysis is described in this paper. The mass scanning circuit contains a new electronic device replacing the mechanically driven scanner which has ever been used. For the analytical works, due emphasis should be given to the maintenance of the overall stability of the instruments for a long period of time. However, some analytical results are reported prior to this routine analysis and also the effects of the electron emitter treatment for the stabilization of the sensitivity and the cracking patterns (mass spectra) are discussed.

Constructive Description of the Instrument

The general schematic diagram of the whole instrument is shown in Fig. 1. It is composed of five unit parts; (1) the gas sampling unit with the proper evacuating unit; (2) the ion producing and accelerating unit; (3) the analyzing part with the magnet current controlling unit; (4) the ion detecting, amplifying and recording system; (5) the main evacuating unit and the emergency protecting equipment. Description is made in detail about each unit part in the following paragraphs.

(1) The Gas Sampling Device

The piping diagram of the gas sampling unit is schematically illustrated in the right part of the Fig. 1. Gas sample contained in the sample bottle is introduced into the sampling pipet of about 2 cc capacity under the adequate pressure which is read on the closed-end mercury manometer. The whole sampling unit must be previously evacuated to the degree of about 1×10^{-5} mm Hg. The pipetted sample is expanded into the gas reservoir of about 3 litre capacity, and then it is introduced to the ionization chamber through the gas-leak. The pressure of the sample after it is expanded into the reservoir is not measured presently. As to the gas-leak, two types are considered. One is a diffusion type and the other is an effusion type. As

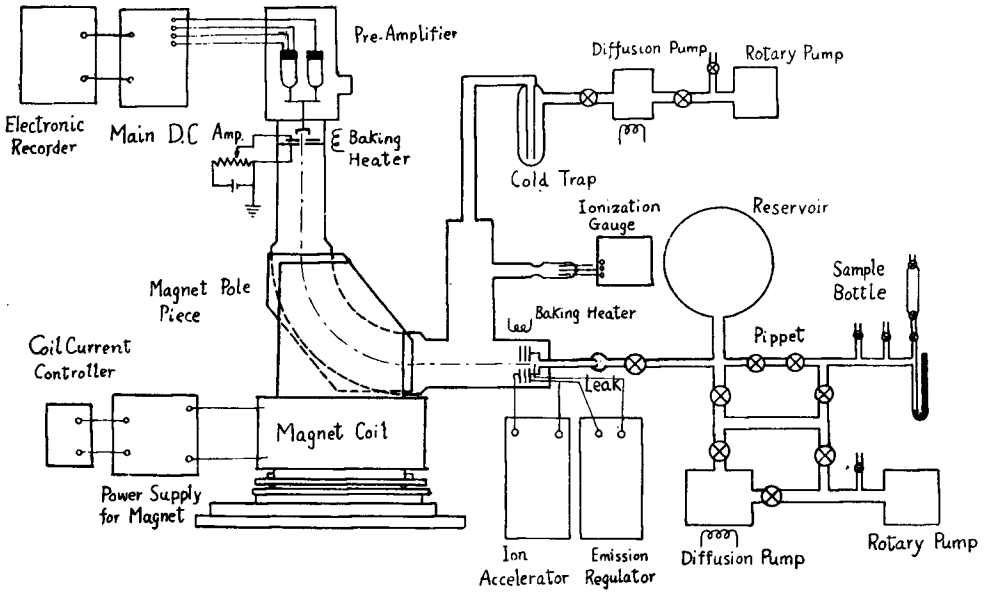

Fig. 1. Schematic diagram of the whole instrument.

for the diffusion type gas leak, a slightly crushed medical injector-needle of ¼ mm diameter was tentatively applied, which proved to possess slightly mass discrimination effects. So the effusion type gas-leak, shown in Fig. 2, is presently used. This is made by grinding off the molten end of a glass tube to the extent that a pin hole of about $^1/_{50}$ mm diameter is obtained. This gas-leak is effective for the usual gas analyzing process, because it shows almost no mass discrimination effect even for the gas mixture containing hydrogen as its main component.

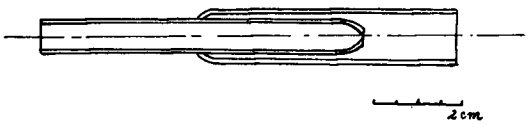

Fig. 2. Gas-leak.

(2) The Ion Source and the Related Circuits

The sectional view of the ion source is shown in Fig. 3 A, and the arrangement of the electron emitting filament, the ionization chamber, the electron trap, and all the electrodes are shown in Fig. 3 B. The electron beam emitted from the filament is defined by the slit (0.5 mm × 6.0 mm) of the ionization chamber. The ionization chamber and all the electrodes are made of molybdenum plate of 0.5 mm thickness, and the filament is a tungsten straight wire (not thoriated) of 0.07 mm diameter and

is set 2 mm apart from the slit. The electrode P_1 draws the positive ions out, so it is usually kept negative to the ionization chamber by several volts. P_2 and P_3 are kept separate in two plates and they compose a focusing lens of the ion beams, and the suitable negative potentials are applied to each plate for the ionization chamber so that the ion beams will be collimated on the slit of the earth potential electrode P_4.

The electric circuit for the ion source can be divided into two parts: (1) the electron emission regulator, and (2) the ion accelerator. These two units combined together are shown in Fig. 4. As to the emission regulator illustrated in the upper part of the figure, the working principle of it is much the same as that proposed by Nier[1] in 1947 with slight differences in the circuit elements. The intensity of a specific emission current is regulated by changing R_9 in the range of between 200μA and 600μA. The regulation is in the range of $\pm$0.1% after the stationary

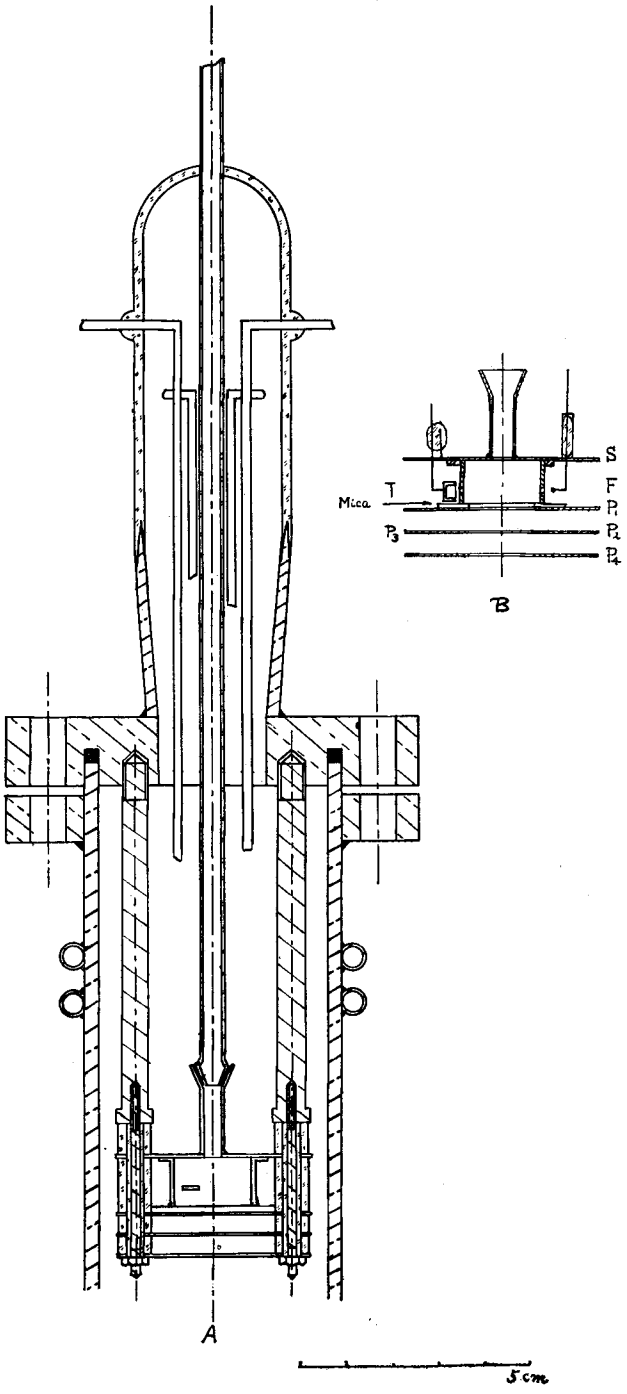

Fig. 3. Ion source.

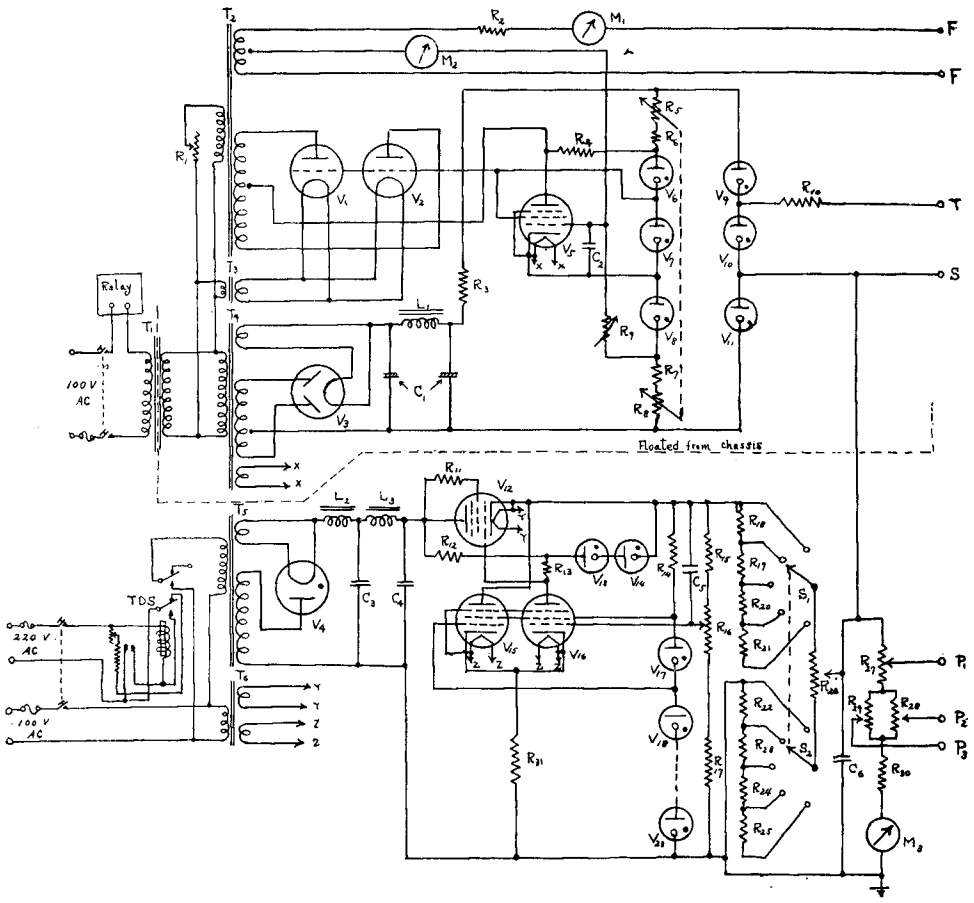

Fig. 4. Stabilized power supply for ion source.
(Emission regulator and ion accelerator)

R_1	200 ohm Slide-ohm		
R_2	4 ohm Wire-wound		
R_4	10 kilo-ohm		
R_4	500 kilo-ohm		
R_5, R_8	10 kilo-ohm Ganged		
R_6, R_7	500 ohm		
R_9	500 kilo-ohm Carbon variable		
R_{10}	20 kilo-ohm		
R_{11}	15 kilo-ohm		
R_{12}	20 kilo-ohm		
R_{13}	1 meg-ohm		
R_{41}	180 kilo-ohm		
R_{15}	1.5 meg-ohm		
R_{16}	500 kilo-ohm Carbon potentiometer		
R_{17}	3 meg-ohm		
R_{18}~R_{25}	80 kilo-ohm		
R_{26}	15 kilo-ohm Wire-wound potentiometer		
R_{27}	1 meg-ohm		
R_{27}, R_{29}	1 meg-ohm Ganged carbon potentiometer		
R_{30}	8 meg-ohm		
R_{31}	500 kilo-ohm		
C_1	8 microfarad	600 V.	
C_2	0.1 microfarad	1000 V.	
C_3	4 microfarad	10000 V.	
C_4	4 microfarad	5000 V.	
C_5	0.5 microfarad	5000 V.	
C_6	2 microfarad	8000 V.	
V_1, V_2	2A3		
V_3	80		
V_4	866 A		
V_5	6 SJ7		
V_6~V_{10}	VR 75		
V_{11}	VR150		
V_{12}	42		
V_{13}, V_{14}	neon lamp		

V_{15}, V_{16}	6SJ7	L_1	30 H 100 mA.
V_{17}~V_{23}	neon lamp	L_2, L_3	30 H 30 mA.
T_1	1:1 Insulation transformer secondary insulated to 2000 V. 200 watt	M_1	0–10 A AC
		M_2	0–1 mA DC
T_2	300-0-300 V 120 mA, 6.3 V 10 A	M_3	0–200 microampere DC
T_3	2.5 V 5 A	TDS	Time-delay-switch adjustable 20–40 sec.
T_4	450-0-350 V 100 mA, 5 V 2 A, 6.3 V 2 A.	S_1, S_2	Ganged
		Relay	cf. Fig. 16.
T_5	0–2000 V 30 mA, 2.5 V 5 A.		
T_6	6.3 V 1 A, 6.3 V 1 A.		

state is reached. R_5 and R_6 are the ganged rheostats which act in a "put and take" manner and the accelerating potential of the emitted electron can be changed; and it can also be stable in the range of between 0 and 70 volts by adjusting these ganged rheostats. Practically, however, the electrons are accelerated in the range of from 50 to 70 volts.

The lower part of the circuit is the usual *D*-type constant voltage supply, the stability of which is promoted by the differential amplifier. S_1 and S_2 are ganged, which compose the voltage selector. It gives four fundamental voltage ranges of 500, 750, 1,000, and 1,250 volts, and R_{26}, prepared for the fine adjustment of the voltage, covers all the ranges of between 300 and 1,300 volts inspite of the stepwise jump of the voltage by S_1 and S_2. The stability of this supply is assured in the range of $\pm 0.01\%$ under normal working conditions.

(3) The Analyzing Part and the Related Circuits

(a) The Analyzer Tube

The analyzing tube is made of a copper tube of 56 mm outer diameter. It is bent to open the angle of $\pi/2$ and has the central radius of 138 mm, and is flattened to the thickness of 20 mm at the analyzing part so as to be held in the gap of the electromagnet, whose clearance is 21 mm. The ion source unit and the ion collector unit are accurately and tightly connected to each end of the tube, and the vacuum system is attached at the branched tube on the ionizing side. All connections are Wilson-sealed, having the synthetic rubber packings. The analyzer tube is wound by 300 watt electric heater wires around the ion source part and the collector part, so that the gas adsorbed on the inner surface of it will be baked out before the performance of the experiment.

(b) The Electromagnet

Fig. 5 shows the electromagnet employed in the authors' case. The purification of the material and the casting of the core was made by Nippon Stainless Steel Co.

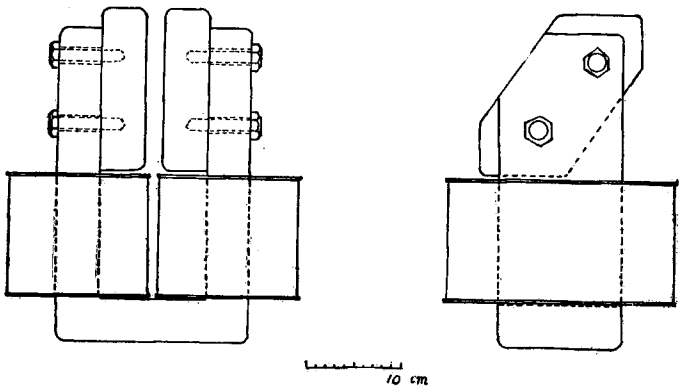

Fig. 5. Electromagnet.

The impurity components analyzed by the maker is shown in Table 1.

Table 1. Impurities in the Core Material.

Element	C	Si	Cr	Mn	P	S	Cu
%	0.03	0.08	0.08	0.13	0.003	0.010	0.23

Total winding of the exciting coil is 51,130 turns of enamelled copper wire of 0.5 mm diameter, and the dc resistance of it is 3,570 ohms. The pole surface is about 200 cm^2 and the air gap is 21 mm. The residual magnetic flux density at the current

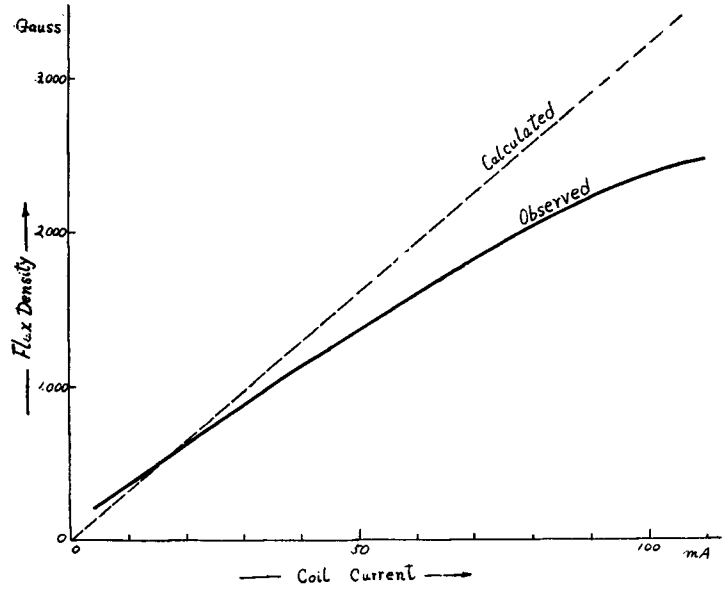

Fig. 6. Characteristic curve of the electromagnet.

distinction after excitng to about 2,500 gauss was as small as 17.4 gauss and this is sufficient to cover the low mass number range with 1,000 volt acceleration. Fig. 6 shows the relation between the coil current and the measured flux density of the magnet compared with that of the ideal magnetization expected from ampere-turn values.

(c) The Electromagnet Supply and the Current Controlling Device

When the magnetic scanning is adopted, it is necessary for the power supply circuit to be designed so as to get the exciting current to increase almost proportionally to the square root of time, from the well-known relation given by the following equation;

$$M/e = 4.82\times10^{-5}\frac{r^2H^2}{V}, \qquad (1)$$

where M is mass number, e charge number, r rotating radius of ion beam in cm, H magnetic flux in gauss, and V accelerating voltage in volt. Thereby the rate of scanning becomes constant, which facilitates the identification of the mass spectra recorded.

To satisfy approximately the conditions above mentioned, several reports have been made by other authors,[2),3)] and some of them were followed by the present authors. But those circuits reported were not always satisfactory; the lower limit of the output current can hardly be diminished without changing the square-root of time proportionality relation in any means. In addition to this fact, the mechanical driving of the scanning circuit in such a power supply has two weak points. The one is that the precise wire wound rheostat employed for scanning is usually too fragile to repeat the scanning with it so many times. The other is the possibility of incomplete scanning or outscanning probably caused by the unstability of the contact at the contact point of the rheostat.

To avoid these weak points which are fatal to the circuit, the authors modified the part of the circuit elements in two points. For the convenience of comparison, a typical example of the previous circuit and the modified one are shown in Figs. 7 and 8, respectively. As to the circuit shown in Fig. 8, the reports are made in other papers,[4),5)] and the detailed illustration about the working principle will not be repeated here. To be brief, C_7 is charged by closing S_3, and the coil current is set at the initial minimum value. By opening S_3, C_7 begins to discharge through the diode part of V_{18} and R_{29} and the scanning begins accordingly. Figs. 9 and 10 show the effect of the existence of the diode on the increase of the coil current close to the postulated time-current relation. Fig. 9 shows the effect of the plate voltage E_p of the diode on the rate of increase of the coil current. The effect of the diode is clearly seen in this figure. Fig. 10 shows the effect of the plate resistance R_{28} directly

connected to the diode on the shape of the scanning rate curve. Fig. 11 shows the relation between the values R_{29} and the scanning rate. The scanning circuit has worked without any difficulties and proved to be of practical use for about two years. One thing remained is the comparatively low value of the upper limit of the coil current owing to the characteristics of the cathode follower V_{18}. But it is not the general difficulty of the circuit of this type. Its smoothness and durability are sufficient enough to substitute the former type supply.

For the purpose of the manual scanning, the extreme right part of the circuit is plugged in through the consent, S_2 is opened, and the scanning is performed by changing R_{32} (coarse) and R_{33} (fine). This device is convenient in the fine collimation of the fixed ion beam by making the electromagnet move slightly or adjusting the potentials on the various electrodes in the ion source.

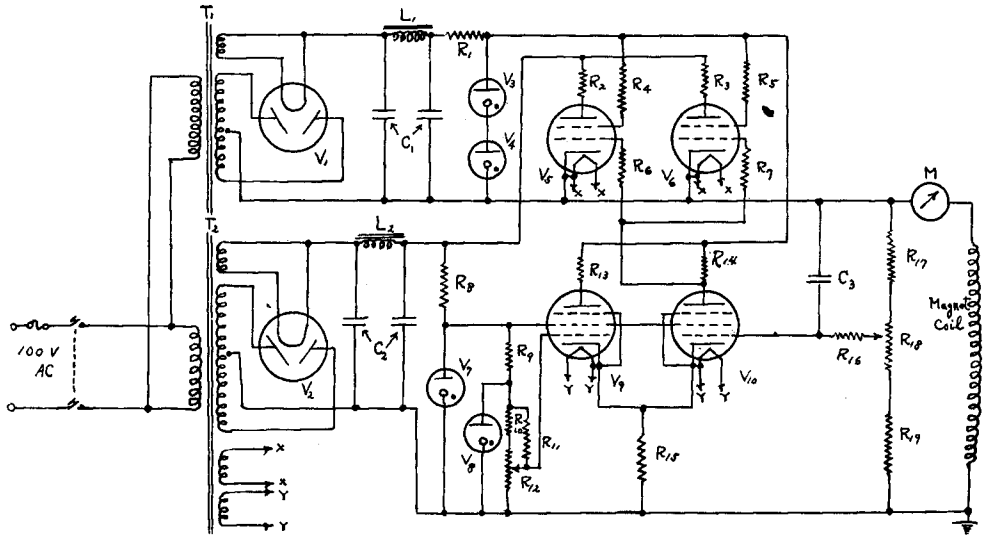

Fig. 7. Stabilized power supply for magnet (No. 1)

R_1	1 kilo-ohm	C_2	8 micro-farad 1000 V
R_1, R_3	100 ohm	C_3	0.5 micro-farad 1000 V
R_4, R_5	1 kilo-ohm	V_1	80
R_6, R_7	100 ohm	V_2	5Z3
R_8	7.5 kilo-ohm	V_3, V_4	VRB 135/60
R_9	5 kilo-ohm	V_5, V_6	807
R_{10}	3.2 kilo-ohm	V_7	VRB 135/60
R_{11}	11.2 kilo-ohm	V_8	VRB 65/60
R_{12}	30 kilo-ohm Wire-wound potentiometer	V_9, V_{10}	6 SJ7
R_{13}, R_{14}	1 meg-ohm	T_1	400–0–400 V 80 mA, 5 V 2 A
R_{15}	30 kilo-ohm	T_2	500–0–500 V 250 mA, 5 V 3 A, 6.3 V 2 A, 6.3 V 2 A
R_{16}	200 kilo-ohm	L_1	30 H 80 mA
R_{17}	100 kilo-ohm	L_2	30 H 250 mA
R_{18}	100 kilo-ohm Carbon potentiometer	M	0–250 mA
R_{19}	50 kilo-ohm		
C_1	4 micro-farad 1000 V		

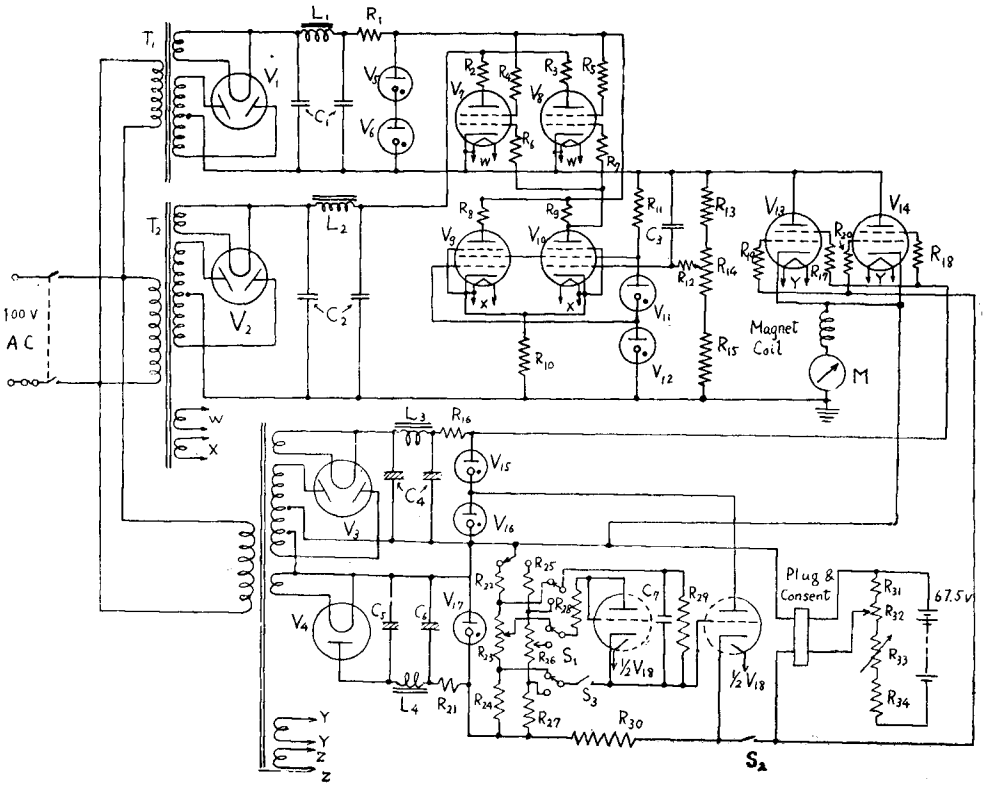

Fig. 8. Stabilized power supply for Magnet (No. 2)

R_1	1 kilo-ohm	C_1	4 micro-farad 1000 V
R_2, R_3	100 ohm	C_2	8 micro-farad 1000 V
R_4, R_5	1 kilo-ohm	C_3	0.1 micro-farad 1000 V
R_6, R_7	100 ohm	C_4	20 micro-farad 450 V
R_8, R_9	1 meg-ohm	C_5	8 micro-farad 450 V
R_{10}	130 kilo-ohm	C_6	40 micro-farad 450 V
R_{11}	30 kilo-ohm	C_7	56 micro-farad 1000 V
R_{12}	500 kilo-ohm	V_1	80
R_{13}	80 kilo-ohm	V_2	5 R4WGY
R_{14}	10 kilo-ohm Carbon potentiometer	V_3	80
R_{15}	10 kilo-ohm	V_4	80 HK
R_{16}	4 kilo-ohm	V_5, V_6	VRB 135/60
R_{17}, R_{18}	2 kilo-ohm	V_7, V_8	807
R_{19}, R_{20}	1 kilo-ohm	V_9, V_{10}	6 SH7
R_{21}	5 kilo-ohm	V_{11}	VR 150
R_{22}	1 kilo-ohm	V_{12}	VR 105
R_{23}	3 kilo-ohm Carbon potentiometer	V_{13}, V_{14}	807
R_{24}	3.75 kilo-ohm	V_{15}	VR 150
R_{25}	1 kilo-ohm	V_{16}	VR 105
R_{26}	2 kilo-ohm Carbon potentiometer	V_{17}	VR 75
R_{27}	4.75 kilo-ohm	V_{18}	6S L7
R_{28}	500 kilo-ohm	T_1	400–0–400 V 100 mA, 5V 2A
R_{29}	8 meg-ohm	T_2	750–0–750 V 180 mA, 5 V 3 A, 6.3 V 2 A 6.3 V 2 A
R_{30}	35 kilo-ohm		
R_{31}	60 kilo-ohm	T_3	300–0–300 V 60 mA, 0–180 V 50 mA, 5 V 2 A, 5 V 0.7 A, 6.3 V 2 A, 6.3 V 2 A
R_{32}	200 kilo-ohm Wire-wound potentiometer	M	0–150 mA DC
R_{33}	5 kilo-ohm Wire-wound variable	S_1	Ganged
R_{34}	130 kilo-ohm		

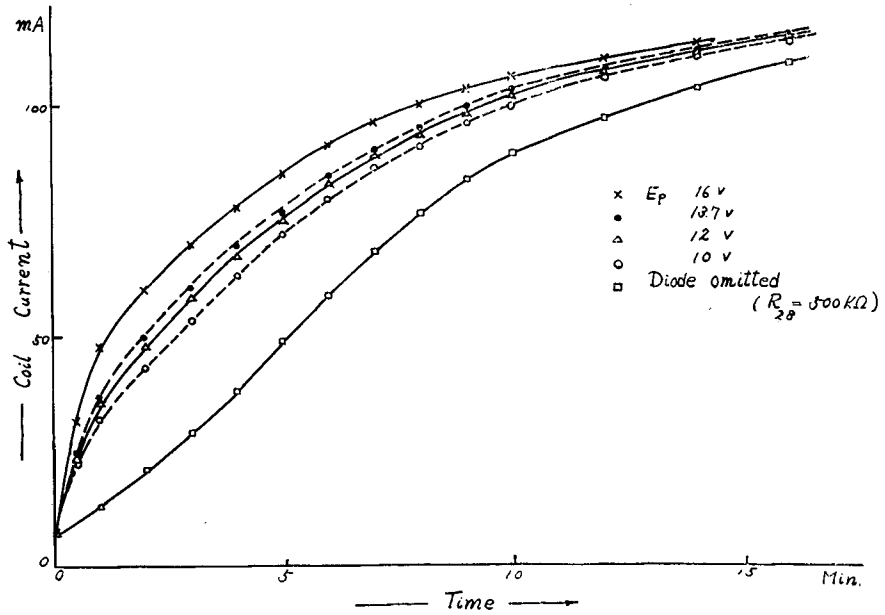

Fig. 9. Relationship of coil current to time for various plate-voltages E_p of diode.

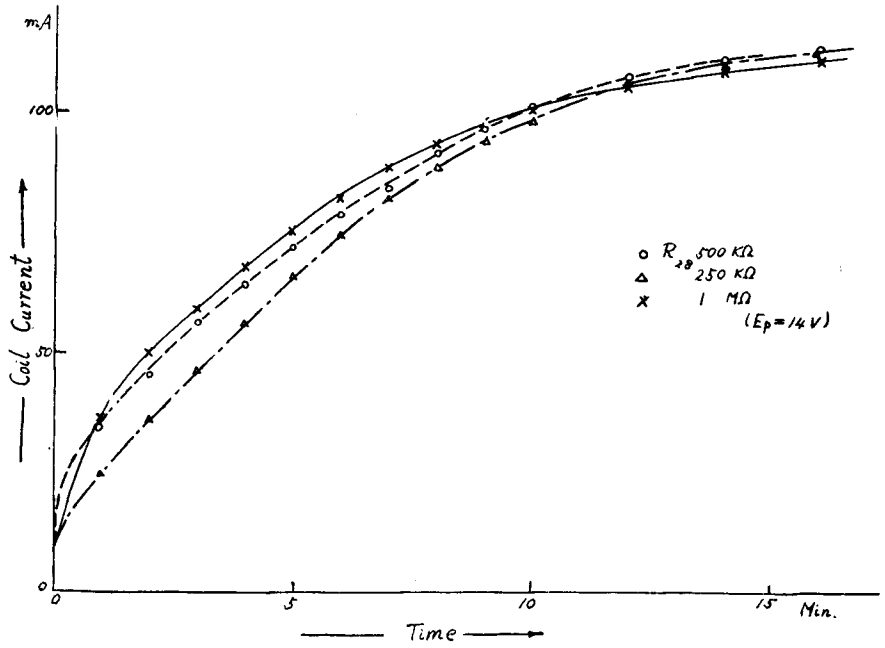

Fig. 10. Relationship of coil current to time for various plate-resistance R_{28} of diode.

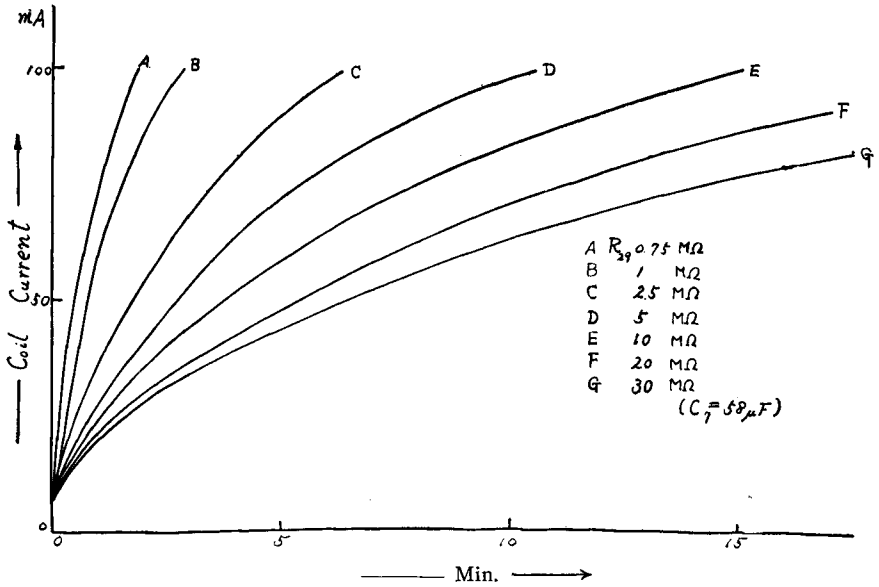

Fig. 11. Relationship of coil current to time for various R_{29}.

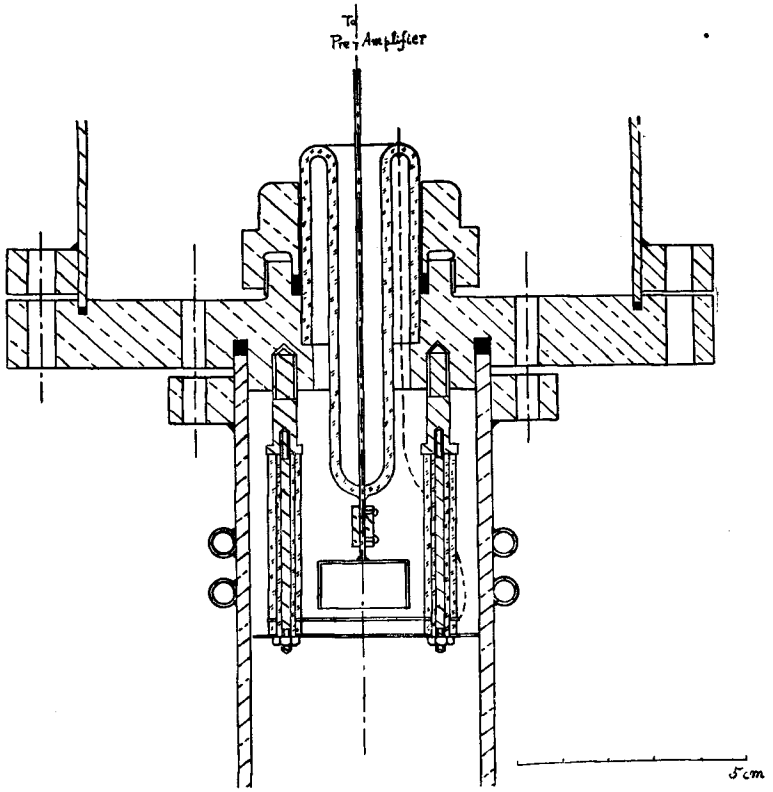

Fig. 12. Ion collector.

(4) Ion Collector and the Ion Current Amplifier

(a) Ion Collector

The sectional view of the ion collector is shown in Fig. 12. It consists of two beam-defining electrodes and the Faraday cage, both of which are made of molybdenum plate of 0.5 mm thickness. Of the two electrodes, the one nearer to the case is kept positive to the earth potential by 40~50 volts in order to act as the secondary electron limiter, and the farther earth potential one, having the diameter nearly equal to the inner diameter of the analyzer tube, seems to act also as the limiter to a certain extent. Otherwise, the secondary electrons which jump into the collector through the slits cause a sudden shift on the balance of the amplifier, appearing on the recorder chart as the peaks in the negative direction.

(b) The Amplifier

The circuit of the ion current amplifier is shown in Fig. 13. The pre-amplifier part is the same one as the balanced circuit originally proposed by Barth,[6] whose UX-54 A tube and the high grid resister of about 10^{10} ohms (both are Toshiba Elec.

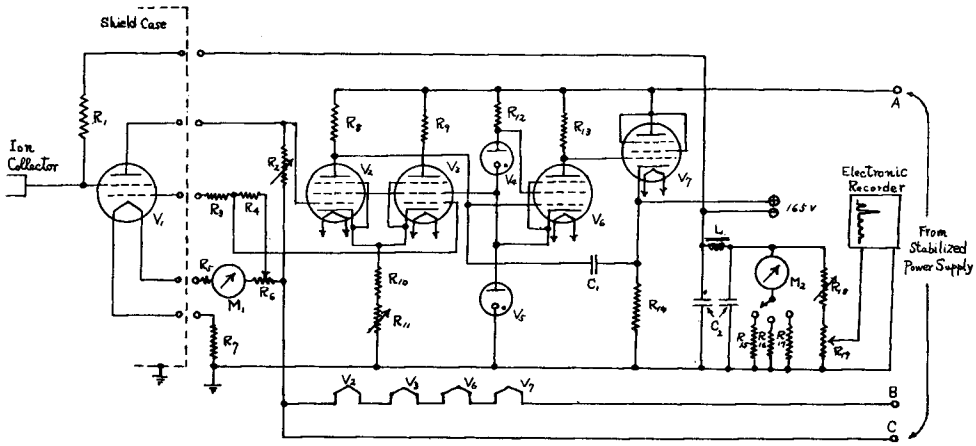

Fig. 13. Pre- and main amplifier.

R_1	10^{10} ohm (Film-resister)	R_{17}	10 kilo-ohm
R_2	30 kilo-ohm Carbon variable	R_{18}	1 kilo-ohm Carbon variable
R_3	10 kilo-ohm	R_{19}	10 ohm Carbon potentiometer
R_4	1 kilo-ohm	C_1	0.002 micro-farad, 2000 V
R_5	7 ohm Wire-wound	C_2	16 micro-farad, 1000 V
R_6	30 ohm Wire-wound potentiometer	V_1	UX 54A
R_7	20 ohm Wire-wound	V_2, V_3	12 SJ7
R_8, R_9	1 meg-ohm	V_4	VR 150
R_{10}	30 kilo-ohm	V_5	VR 105
R_{11}	10 kilo-ohm Carbon variable	V_6, V_7	12 SJ7
R_{12}, R_{13}	1 meg-ohm	L	30 H 60 mA
R_{14}	30 kilo-ohm	M_1	0-250 mA DC
R_{15}	2 meg-ohm	M_2	0-100 microampere DC
R_{16}	100 kilo-ohm		

Co. made) are enclosed in the iron made schielded box, which is directly connected to the lead from the ion collector. They are jointed by the consent to the other part of the amplifier at the place shown by the dotted line in Fig. 13. The main amplifier is, as shown in the figure, a 100% inverse feed back amplifier and its voltage gain is unity. The output is fed to the recorder or read on the meter (100μA) through the

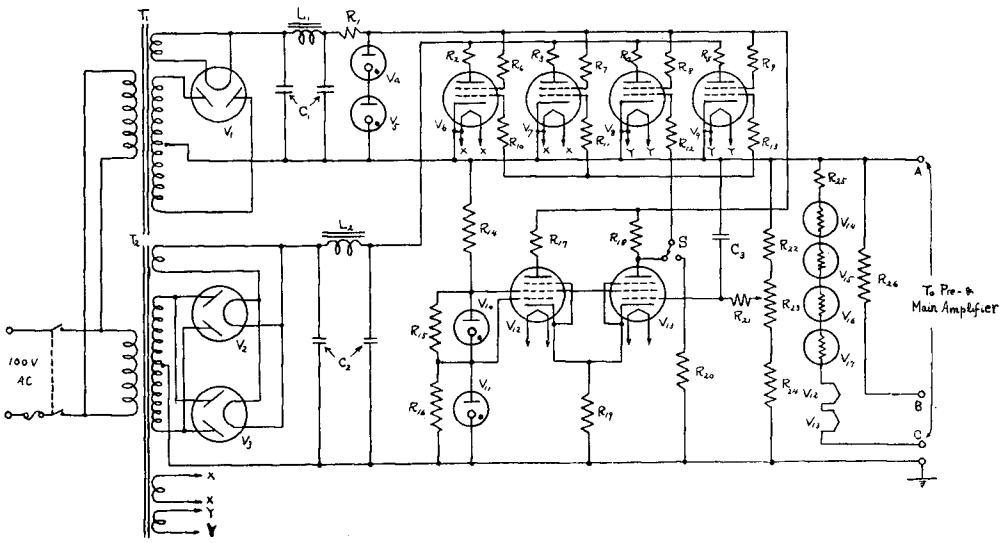

Fig. 14. Stabilized power supply for amplifier.

R_1	2.5 kilo-ohm	C_2	16 micro-farad 1000 V
R_2~R_5	1 kilo-ohm	C_3	0.5 microfarad 1000 V
R_6~R_9	100 ohm	V_1	80
R_{10}~R_{13}	100 ohm	V_2, V_3	5Z3
R_{14}	2 kilo-ohm	V_4, V_5	VRB 135/60
R_{15}	50 kilo-ohm	V_6~V_9	807
R_{16}	250 kilo-ohm	V_{10}	VR 150
R_{17}, R_{18}	1 meg-ohm	V_{11}	VRB 65/60
R_{19}	100 kilo-ohm	V_{12}, V_{13}	12 SJ7
R_{20}	750 kilo-ohm	V_{14}~V_{17}	B-37
R_{21}	250 kilo-ohm	T_1	400-0-400 V 100 mA, 5 V 2 A
R_{22}	75 kilo-ohm	T_2	550-0-550 V 300 mA, 5 V 3 A, 6.3 V 2 A, 6.3 V 2 A.
R_{23}	10 kilo-ohm Wire-wound potentiometer	L_1	30 H 100 mA
R_{24}	20 kilo-ohm	L_2	10 H 300 mA
R_{25}	125 ohm	S	Time-delay-switch for control
R_{26}	7 kilo-ohm		
C_1	8 micro-farad 1000 V		

cathode follower V_7 and then the filter net work. As the power supply of the dc amplifier, a *D*-type stabilizer with the differential amplifier is employed as shown in Fig. 14. The stability of the power supply is about 0.02% against the change of 100 ± 5 volts in the ac line voltage.

(App.) UN-954 Electrometer Circuit[7]

Recently tendency in the dc amplifier for detecting the minute current is to spare the expensive UX-54 tube. The authors had constructed an amplifier using acorn tube 954, of which the publication was made. Fig. 15 shows that schematic circuit elements, however, the *D*-type stabilizer is replaced by a suitable ac stabilizer here because such a dc stabilizer is as expensive as the electrometer tube. The 954 tube is moulded into a sulphur block to diminish the grid leakage caused by the surface conduction and a pretty good results are obtained.

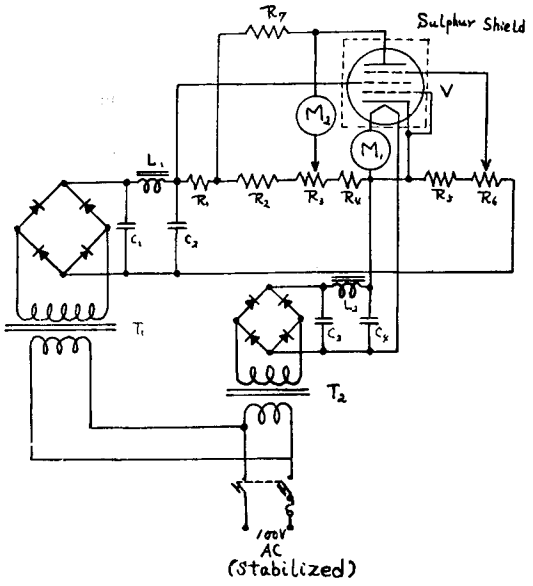

Fig. 15. 954 Electrometer circuit.

R_1	5 kilo-ohm	C_3, C_4	1000 micro-farad 20 V
R_2	3 kilo-ohm	V	954
R_3	1 kilo-ohm Wire-wound potentiometer	L_1	20 H 30 mA
R_4	11 kilo-ohm	L_2	5 H 150 mA
R_5	6 kilo-ohm	T_1	0-16.5 V 30 mA
R_6	600 ohm Wire-wound potentiometer	T_2	0-6.3 V 150 mA
R_7	50 kilo-ohm	M_1	0-200 mA DC
C_1	200 micro-farad 50 V	M_2	-5-0-5 microampere DC
C_2	100 micro-farad 50 V		

(5) The Vaccum Unit and Safety Equipment

The vacuum unit is constructed as schematically shown in Fig. 1. The vacuum gauge employed is the usual Fogel type ionization gauge, of which the detailed description is omitted. The fore vacuum pump is a dual type rotary vacuum pump of 5 cdm/min displacement. The main diffusion pump is of oil diffusion type with the

pumping speed of 120 litres/sec. giving the guaranteed end vacuum of 5×10^{-7} mm Hg with the blind end. A cold trap cooled by the dry ice-ethyl alcohol cold mixture is employed between the analyzer tube and the diffusion pump. The stationary vacuum depth of 3×10^{-6} mm Hg at the analyzer tube is realized under the ordinary working conditions. The running of the instrument must be maintained ceaselessly in order to get the stationary condition for the routine work of analysis. For emergencies which may occur at any time, the safety equipments are indispensable to the instrument, and it is shown in Fig. 16. In the case of the electric current stopping, the

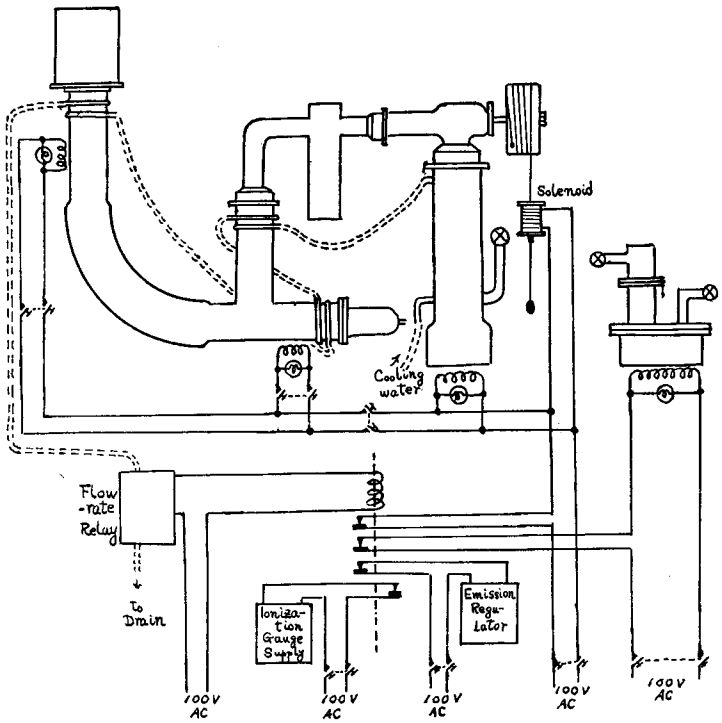

Fig. 16. Safety equipments.

stop valve on the diffusion pump is closed by gravity and all the electric circuits are cut off and do not act before resetting the magnet switch. When the water supply stops or goes down to the dangerous flow rate, the same protecting actions are made as above and the emergency buzzer or lamp circuit comes to be closed. Against the sudden lowering of the vacuum depth to the dangerous state, the safety device is not yet equipped, however, under the ordinary electric and water supply conditions, such a case is very scarce.

The front-view of the mass spectrometer is shown in the photograph.

Experimentals

Three factors are important to estimate the characteristics of the mass spectrometer: (1) resolving power, (2) stability of sensitivity, and (3) stability of the cracking pattern. Discussions are made about the each factor in the following paragraphs.

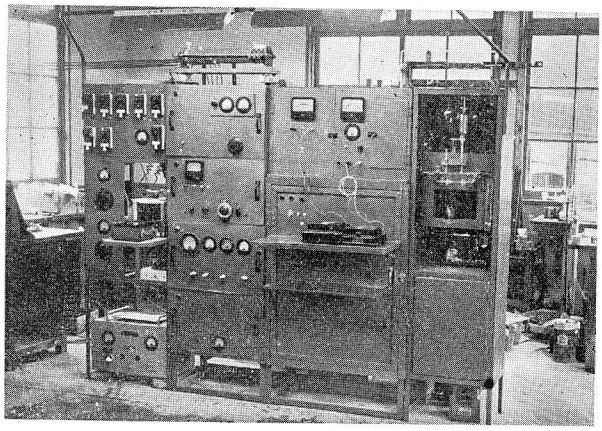

General view of the mass spectrometer.

(1) Resolving Power

The ideal resolving power based on the absolute dimension of the instrument, provided that all the other conditions are ideal, is simply defined by the equation,

$$\text{Resolving power} = \frac{r}{d_1+d_2}, \qquad (2)$$

where r is the radius of curvature of the magnetic field, and d_1 and d_2 are widths of the ion exit slit in the ion source and the ion entrance slit in the ion collector, respectively. In the authors' case, $r = 138$ mm, $d_1 = 0.5$ mm, and $d_2 = 1$ mm, which give the resolving power of 92.

Though the various methods of defining the actual resolving power are proposed, it is usual that the actual resolving power is lower than that expected from the eq. (2) because of the geometrical incompleteness in the optical construction. To estimate the actual resolving power, an example of the cracking pattern of *n*-Butane[8] is shown in Fig. 17. When the resolving power is determined by the half-width method, which is most popularly adopted, the mean value becomes about 90 which is close to the theoretical value. The overlapped parts seen in the feet of the two adjacent peaks are indeed due to the metastable ions, which are shown in the figure with the processes of producing them.

(2) Stabilities of Sensitivity and Cracking Patterns

Though the absolute value of the sensitivity, by which the efficiency of the instrument is estimated, is an important characteristics, the most serious problem is the stableness of the sensitivity and consequently of the cracking pattern as the relative values of the sensitivity. In the case of the quantitative analysis, stability of these factors are indispensable by every means.

To get the good stabilities of sensitivity and cracking pattern, the outer conditions

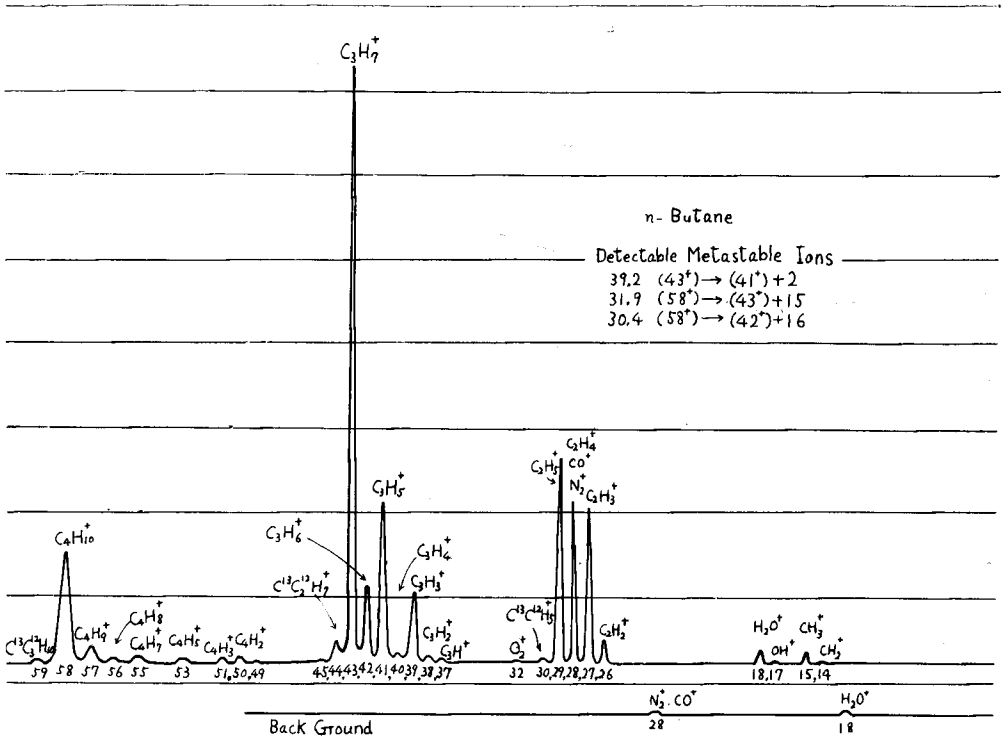

Fig. 17. Cracking pattern of *n*-butane.

for the production of the parent and fragment ions must be kept strictly constant. Though it is clear that the structure of the ion source is highly related, the temperature on the ionization chamber wall, the velocity distribution change of the ionizing electrons caused by the charge distribution change in the circumference, and the state of the filament, and the stability of vacuum, combined together, have a great influence on the stability.

Especially the temperature of the ionization chamber and the state of the filament are said to play greater part. For example, the "Isatron" manufactured by the C. E. C. is equipped with the temperature controlling device, having good stability as well as the superiority in the accurateness of construction.

As the chemical method of stabilizing the surface of the filament, a treatment of the filament with unsaturated hydrocarbon (e. g. 1-Butene) at the incandescent state is being appreciated recently.

The effect of the treatment may be considered to be the fact that the surface of the filament is covered with carbon isolated from hydrocarbons, processing the thermal cracking on the surface. If so, the ordinary saturated hydrocarbons are also considered

effective as the treating substance for the stabilization of the filament surface. The authors tentatively treated the filament with *n*-Butane under the following condition.

As in the case of the usual analysis, *n*-Butane is expanded into the reservoir and led to the analyzer with the filament incandescent and emissionless. The pressure of *n*-Butane in the analyzer was kept $4\sim5\times10^{-5}$ mm Hg. As the treatment went on, the resistance of the filament gradually increased, and after the treatment of about 16 hours, it settled at the 110% of the initial resistance and remained almost constant thereafter. The treatment was considered to have come to the end by this time.

Sensitivities and relative sensitivities of *n*-Butane spectra in two sets of series of analysis before (named Series I Experiment) and after (named Series II Experiment) the treatment are shown in Figs. 18 and 19, respectively. As seen from the comparison of these two figures, the stabilities of sensitivity and relative sensitivities are considerably promoted with the appreciable accuracy and reproducibility. Numerically, the mean deviation of the sensitivity decreased to 1.2% in Series II from 6.2% in Series I Experiment.

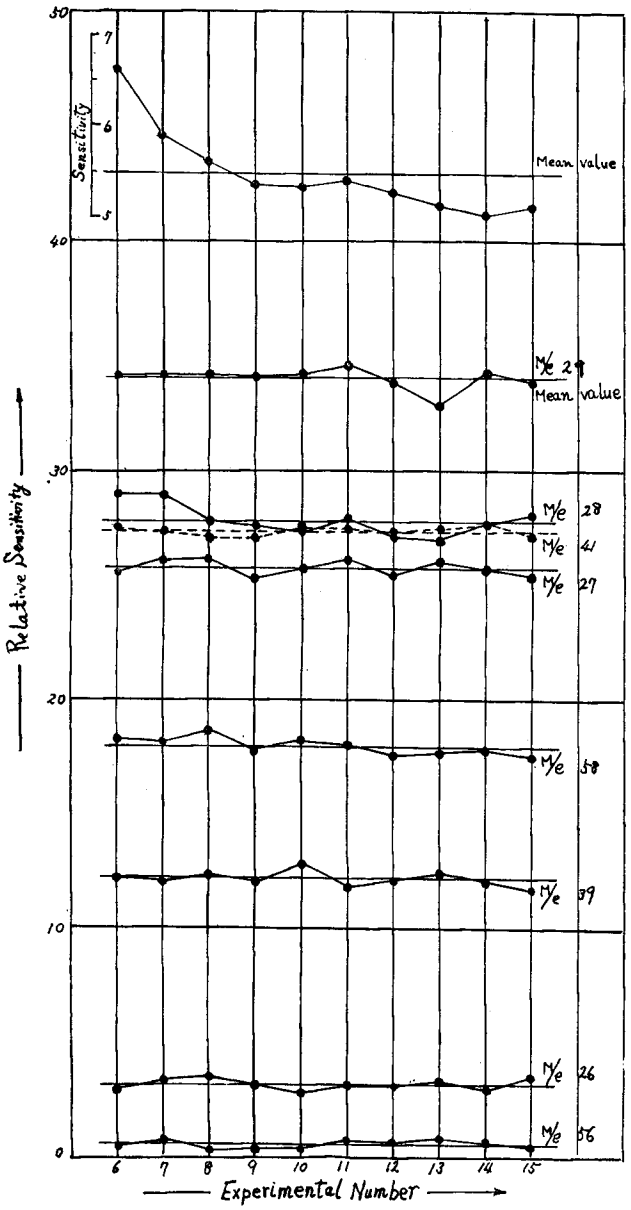

Fig. 18. Stabilities of Sensitivity and Pattern Coefficients of *n*-butane in series I experiments.

The stability of the relative sensitivities, especially of the small peaks, was also bettered. The slight difference in the patterns between Series I and II Experiments is due to the difference in the ion draw out potential between both series. From the results above mentioned, the effect of the treatment of the filament with *n*-Butane is

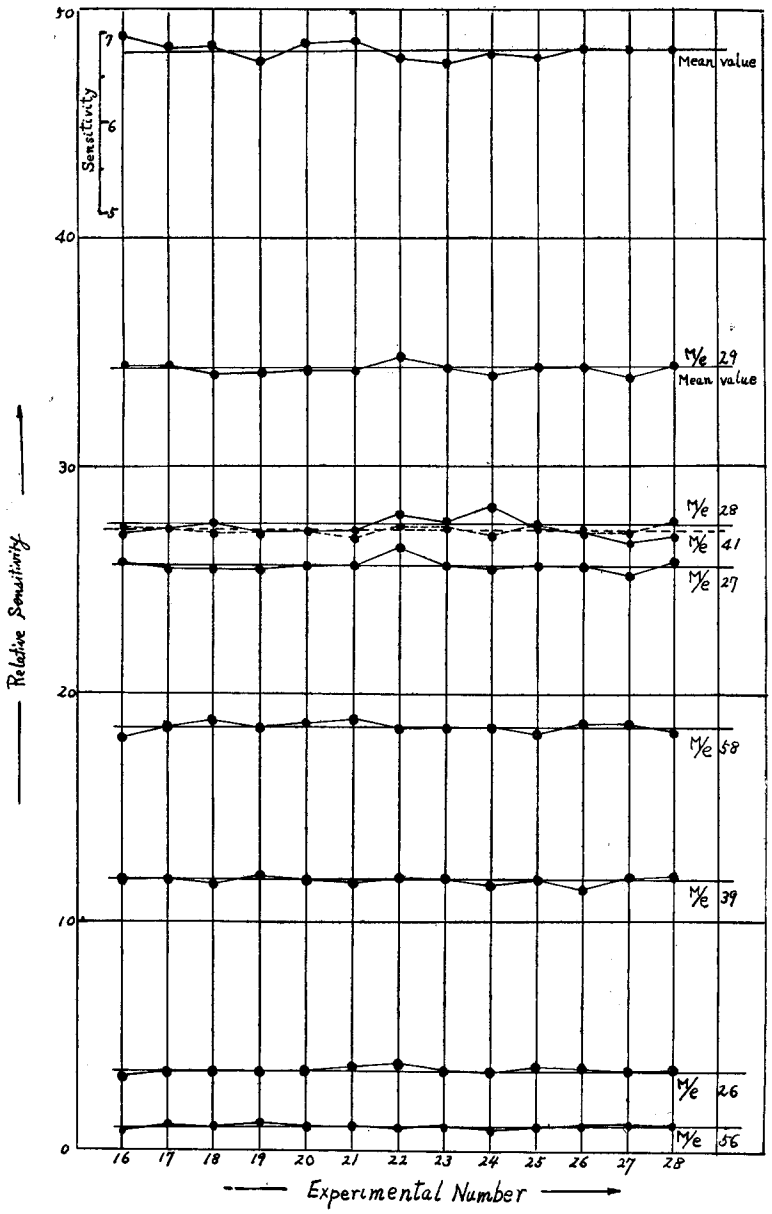

Fig. 19. Stabilities of sensitivity and pattern coefficients of *n*-butane in series II experiments.

affirmed to be effective as the case with unsaturated hydrocarbons.

(3) Analytical Examples

The actual analysis of gas mixture is shown here. The gas mixture analyzed is of four components, which are N_2, H_2, CH_4, and Ar. The ionization efficiencies of them were measured as shown in Table 2, where two literature values are added for reference.

Before the analysis of the industrial gas sample, the synthetic mixture containing the same components as the sample gas was analyzed, which indicated the difference

Table 2. Ionization Efficiency.

Gas	Observed	T. Kambara	L.G. Smith
H_2	1.00	1.00	1.00
H_2	0.72	0.39	0.35
Ar	1.70	1.53	1.30
CH_4	1.27	—	—

Table 3. Mass Spectrometric Analysis.

Component gas	Fresh Gas %	Circular Gas %
N_2	72.7	62.7
H_2	27.2	19.3
Ar	0.1	16.2
CH_4	—	1.8

between the blended ratio (%) in the synthetic mixture and the percentage observed with the mass spectrometer was within one percent. This result obtained served the authors to conclude that the routine analysis were probably capable with the accuracy of about 1 per cent error by using their mass spectrometer. Table 3 gives the analytical results of the fresh gas and the circular gas in a synthetic ammonia plant. Enrichment of argon and methane during the recycling with the separation of the product is seen.

Acknowledgments

For the construction of the mass spectrometer a free contribution of funds amounting to ¥300,000 was made by Befu Chemical Industrial Co., and for the maintenance of the instrument the Scientific Research Fund from the Ministry of Education was shared for three years, to which authors are heartily thankful. The assistance by T. Kanagawa in this work is also deeply appreciated.

Literatures

1) A. O. Nier: Rev. Sci. Instrument, **18**, 398 (1947).
2) T. Kambara: "Symposium on Mass Spectrometry" (The Physical Society of Japan) p. 62 (1950).
3) H. Ezoe: Reports of the Scientific Research Institute, **27**, 435 (1951).
4) N. Kadota, S. Ishida, Y. Masuda and G. Kimura: "Symposium on Mass Spectrometry" (Applied Physical Society of Japan) p. 125 (1954).
5) N. Kadota, S. Ishida and Y. Masuda: Mass Spectrometry, No. 5, 26 (1955).
6) G. Barth: Zeits. f. Phys., **87**, 399 (1934).
7) N. Kadota, S. Ishida and G. Kimura: Chemistry and Chem. Industry, **4**, 248 (1951).
8) This is research grade *n*-Butane from Phillips Petroleum Co.